ADVANCED MATERIALS

Supporting Information

for

Advanced Materials, adma.200601156

© Wiley-VCH 2006
69451 Weinheim, Germany

Supplementary Information

Crosslinked Bicontinuous Cubic Lyotropic Liquid-Crystal/Butyl-Rubber Composites: Highly Selective, Breathable Barrier Materials for Chemical Agent Protection**

By *Xiaoyun Lu*, *Vinh Nguyen*, *Meijuan Zhou*, *Xiaohui Zeng, Jizhu Jin, Brian J. Elliott*,* and *Douglas L. Gin**

Dept. of Chemical & Biological Engineering, and Dept. of Chemistry & Biochemistry, University of Colorado, Boulder, Colorado 80309 (USA)

TDA Research, Inc., 12345 W. 52nd Ave., Wheat Ridge, Colorado 80033 (USA)

Materials. LLC monomers **1** and **2** were prepared according to literature procedures.[1,2] Spectral and chemical purity data were consistent with those described in the literature.[1,2] BR (Butyl 165, 1.2 mol % unsaturation, Mooney viscosity 45) was obtained from the ExxonMobil Chemical Corporation. Solupor® E075-9H01A support was provided by DSM Solutech, The Netherlands. The activated carbon used for CEES trapping and analysis was ANASORB coconut shell charcoal (Cat. No. 226-01) purchased from SKC, Inc. All other reagents and solvents were purchased from commercial chemical suppliers and used as received. All chemical synthesis manipulations were performed under light Ar flush using conventional Schlenk line techniques.

Instrumentation. PLM studies was performed using a Leica DMRXP polarized light microscope equipped with an Optronics digital camera and a Linkam THMSE 600 hot/cold stage

controlled by a Linkam TP92 temperature controller (accuracy: ± 0.1 °C). Powder XRD spectra were obtained using an Inel CPS 120 diffraction system using monochromated Cu K_α radiation. This system was equipped with an Inel programmable capillary oven (accuracy: ± 3°C) for variable-temperature studies. All XRD spectra were calibrated against silver behenate as a diffraction standard (d_{100} = 58 Å), so the accuracy is within 1 Å up to the value of the d-spacings. LLC mixtures were mixed using an IEC Centra-CL2 centrifuge. Element distribution analysis under high magnification was performed using a JEOL 8600 electron microprobe analyzer. Hot-pressing of LLC-BR mixtures was performed using a Wabash Genesis heated platen press. Supported LLC-BR membranes were photo-cured using a Novacure 2100 (EXFO) spot curing apparatus with a rated output of 5,000 mW cm^{-2} (320–500 nm) on a 70 °C hot plate regulated by a WATLOW series 965 temperature controller. UV light fluxes at the sample surface were measured using a Spectroline DRC-100X digital radiometer equipped with a DIX-365 UV-A sensor. ^{1}H NMR spectra were obtained using a Varian Inova 500 spectrometer. FT-IR measurements were performed using a Nicolet MAGNA-IR 760 spectrometer with the samples sandwiched between NaCl crystals.

Preparation and characterization of LLC-BR mixtures and phase diagram determination. **2**–BR composites were prepared by first forming the Q phase of **2** and just water. This was done by weighing appropriate weight percentages of **2** and water into a glass vial, sealing the vial with Parafilm, and alternately hand-mixing and centrifuging (3800 rpm, 10 min) the **2**/water mixture three times at ambient temperature. After confirming formation of the initial **2**/water Q phase by PLM and XRD, the appropriate amount of BR as a 9.1 wt % solution in hexanes was then added to the initial Q-phase mixture. The top of the glass vial was then partially sealed to prevent water loss during further mixing while allowing the hexanes to evaporate away during the hand mixing process. The resulting **2**/BR/H_2O blend was then sealed and alternately hand-mixed and centrifuged (3800 rpm, 10 min) another three times at ambient temperature. The final mixture was equilibrated for at least 16 h before any further testing. The

composition range of each LLC phase was determined using variable temperature PLM. Specimens for PLM analysis were prepared by pressing samples of each different composition between microscope cover-slips. Transitions from one texture to another were recorded on the heating cycle, and were repeated at least three times. The identity of each observed phase was then confirmed by XRD by analyzing a point in each distinct phase region as elucidated by PLM analysis. Specimens for variable-temperature XRD analysis were placed in 1.0 mm I.D. glass capillary tubes using centrifugation to load the LLC mixtures. The **2**/BR/H_2O at ambient temperature showed primarily a L phase (see Figure S1 below). Using these techniques, a partial phase diagram for the **2**/BR/H_2O at 70 ± 5 °C showing the location of the Q phase region was plotted. The LLC phases of some specific compositions at 70 ± 5 °C are listed in Table S1 below. Some XRD and PLM data for some representative compositions with Q, H_I, and L phases are shown in Figure S2 below.

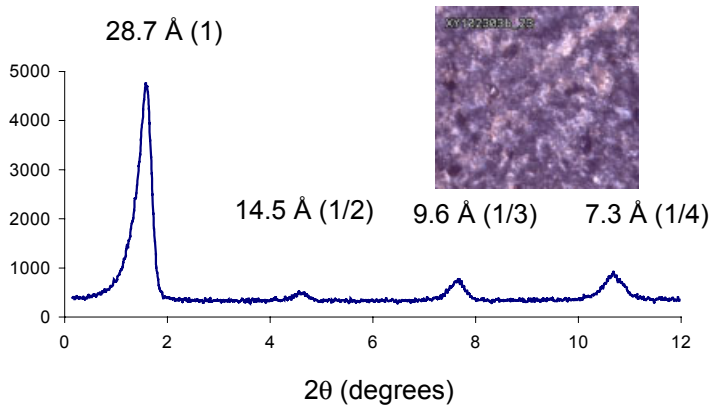

Fig. S1. XRD and PLM data for a L-phase mixture containing 75.3/ 8.2/16.5 (w/w/w) **2**/BR/H_2O at 21 ± 1 °C.

Table S1. Some representative compositions (weight percentage) of **2**, water, and BR that form Q_I, H_I, and L phases at ca. 70 ± 5 °C.*

Monomer 2 (wt %)	Water (wt %)	BR (wt %)	Phase
59.1	31.8	9.1	H_I
61.9	33.3	4.8	H_I
65.7	29.5	4.8	H_I
44.7	19.1	36.1	Q_I
45.4	19.5	35.1	Q_I
48.2	17.9	33.9	Q_I
49.3	21.2	29.5	Q_I
52.8	22.6	24.6	Q_I
53.0	16.8	30.2	Q_I
55.8	23.8	20.4	Q_I
61.4	13.5	25.1	Q_I
62.2	26.7	11.1	Q_I
63.0	27.0	10.0	Q_I
66.4	24.6	9.0	Q_I
71.6	22.5	5.9	Q_I
76.4	14.6	9.0	Q_I
82.0	18.0	0.0	Q_I
86.0	14.0	0.0	Q_I
88.0	12.0	0.0	Q_I
81.9	13.3	4.8	L + (unidentified)
76.4	14.5	9.1	L + (unidentified)

* As can be seen in the yellow highlighted data for comparison, at the same wt % BR in the system, progressively *decreasing* the amount of LLC monomer relative to water causes the system to form first a Q phase and then an H phase. Since these two phases lie on the water-rich side of the L phase, the observed Q and H phases are of the "normal" (i.e., type I) variety. The expected phase progression of L to Q_I to H_I with increasing water content is also consistent with the presence of a Type I Q phase.

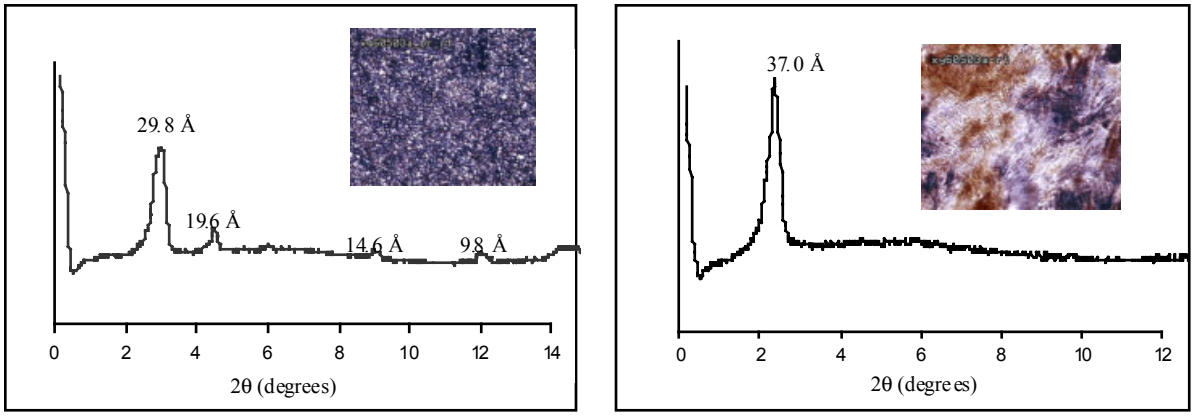

(a) (b)

Fig. S2. XRD and PLM data for (a) a mixture containing 76.4/9.1/14.5 (w/w/w) **2**/BR/H_2O exhibiting a L phase + an unidentified LLC phase; and (b) a mixture containing 59.1/9.1/31.8 (w/w/w) **2**/BR/H_2O exhibiting an H_I phase, both at 70 ± 5 °C.

Electron microprobe analysis (EMA) for P to determine Q-phase 2–BR sample homogeneity. To check if **2** and BR were homogeneously blended in the Q-phase samples, photo-cross-linked samples of the **2**/BR/H_2O mixtures were examined under scanning electron microscopy conditions using an electron microprobe analyzer (EMA) set to detect elemental phosphorus. The distribution and uniformity of elemental P, which is found only in monomer **2**, is a direct measure of how homogeneous the **2**/BR/H_2O mixtures are on the micron scale. Figure S3 shows representative EMA images for P (bright areas) for a cross-linked Q-phase samples that is homogeneously mixed down to the ca. 1 μm level and a sample at the onset of **2**–BR phase separation.

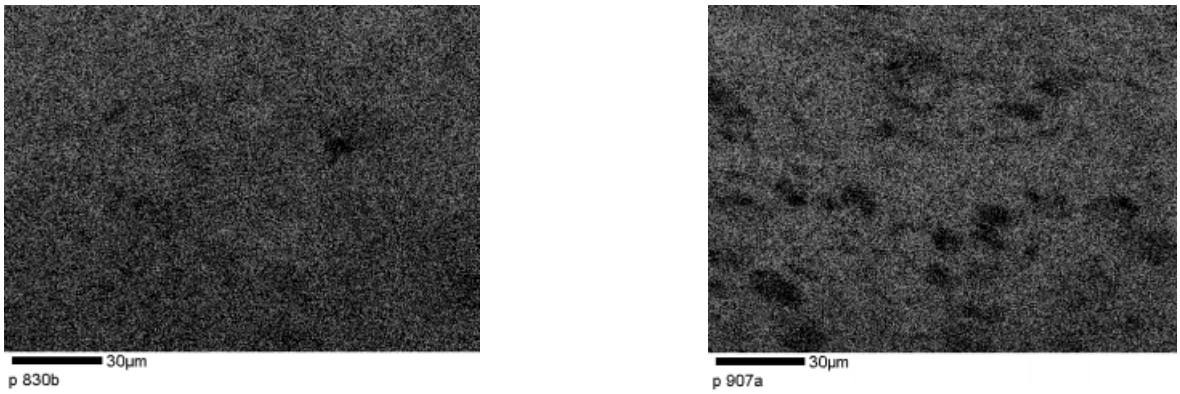

(a) (b)

Fig. S3. Representative EMA images showing elemental P distribution (bright areas) on the surface of cross-linked Q-phase **2**-BR samples: (a) a homogeneously mixed Q-phase sample containing 71.3/13.0/15.7 (w/w/w) **2**/BR/H_2O, and (b) Q-phase sample containing 75.6/20.0/14.4 (w/w/w) **2**/BR/H_2O showing the onset of phase-separation.

It should be noted that when linear polymers such as BR mix with a small molecule additive (a solvent, or in this case, the LLC monomers), an overall negative ΔG_{mix} (leading to formation of a homogeneous solution) or an overall positive ΔG_{mix} (leading to formation of a phase-separated mixture) can result. This depends on the mole fraction and volume fraction of each component in the mixture, according to Flory–Huggins theory for polymer mixing.[3] Thus, changing the relative proportions of the BR polymer, LLC monomer, and water in our system can either generate homogeneous well-mixed samples, or form phase-segregated LLC/BR mixtures at a fixed temperature. Indeed, changing from homogeneous H_{II}-phase LLC-BR blends to phase-separated LLC/BR mixtures have already been observed upon changing the proportions of BR, LLC monomer **1**, and water in a prior publication.[4]

Preparation of photopolymerized, supported Q-phase 2–BR membranes. A small amount of Q-phase LLC-BR paste containing 73.9/9.0/16.2/0.9 (w/w/w/w) **2**/BR/H_2O/photo-initiator was first placed on a piece of Solupor® E075-9H01A support. This material was then

sandwiched between two Mylar sheets and placed between two smooth aluminum plates. The entire assembly was then inserted into a hydraulic press pre-heated to 70 °C. The sample was kept in the heated press for 3 minutes until the initial LLC-BR gel became more fluid, and then 12 tons of force was applied to the composite sample for 5 min to push the fluid LLC-BR mixture into the porous Solupor® support. The resulting infused film (still between Mylar sheets to avoid water evaporation) was then placed between two glass plates, moved to a hot plate regulated to 70 °C, and then irradiated with 320–500 nm UV light (ca. 200 mW cm^{-2} measured at the sample surface) for 15 min to fix the Q-phase microstructure. The LLC phase of the resulting supported LLC-BR film was confirmed by XRD analysis, and the degree of diene polymerization was determined by mid-IR analysis by monitoring the decrease in absorbance of the terminal olefin C-H wagging band at 1004 cm^{-1}. The characteristic strong C–H wagging band of the terminal CH_2=CH– unit of the ω-alkyl-1,3-diene unit was found at 1004 cm^{-1}, based on *trans*-1,3-pentadiene as a model compound (www.sigmaaldrich.com/spectra/ftir/FTIR000274.PDF), and the fact that the C–H wagging band of the terminal CH_2=CH– unit of mono-alkyl substituted olefins is typically found at ca. 990 cm^{-1}.[5] This IR band is lost upon diene polymerization. A picture of a Q-phase **2**/BR/H_2O film hot-pressed and photo-cross-linked into Solupor® is shown in Figure S4 below. Representative mid-IR spectra of an infused Q-phase **2**/BR/H_2O film on Solupor® before and after photopolymerization are shown in Figure S5.

Fig. S4. Picture of a cross-linked Q-phase **2**-BR film made by hot-pressing into Solupor® membrane support.

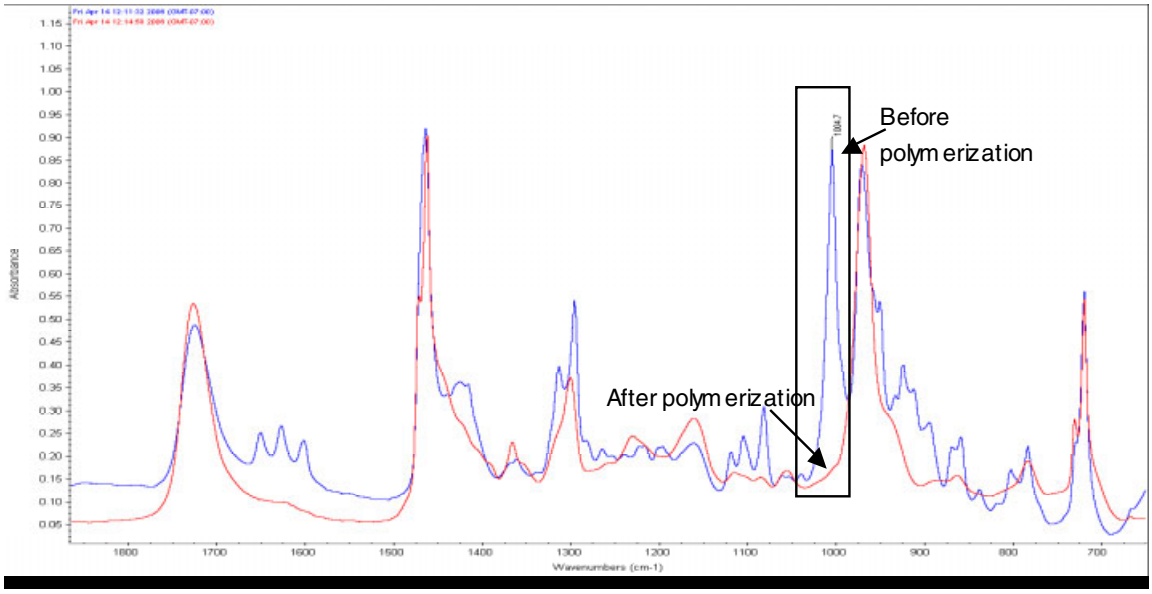

Fig. S5. FT-IR spectra of a hot-pressed Q-phase **2**/BR/H_2O film on Solupor® support (73.9/9.0/16.2/0.9 (w/w/w/w) **2**/BR/H_2O/photo-initiator) before and after photopolymerization, showing greater than ca. 95% 1,3-diene conversion.

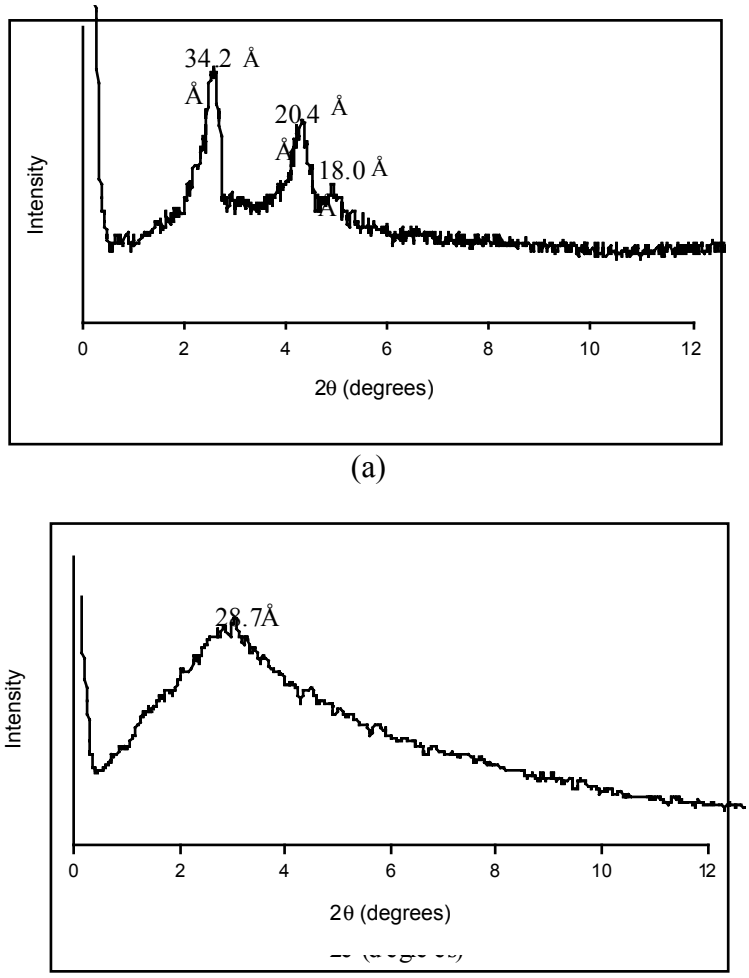

Fig. S6. XRD spectra of (a) an cross-linked H_{II}-phase LLC-BR membrane on Solupor® made with 73.9/16.2/9.0/0.9 (w/w/w/w) **1**/water/BR/photoinitiator by hot-pressing at 50 °C; and (b) a cross-linked L-phase LLC-BR membrane on Solupor® made with 73.9/16.2/9.0/0.9 (w/w/w/w) **2**/water/BR/ photo-initiator by melt infusion at 45 °C.

Preparation of cross-linked, pure BR membranes. Pure cross-linked BR films for permeation comparison purposes were prepared at TDA Research, Inc. by using a low-temperature vulcanization procedure without any additives such as mold releasing agents, stabilizers, or fillers. Exxon Butyl 165 (50.0 g), was combined with tetramethylthiuram disulfide (TMTDS) (1.0 g), and 4,4'-dithio-bis-morpholine (DTDM) used as thermal cross-linking agents.

TMTDS was obtained from Flexsys, and DTDM was obtained from Alfa Aesar. The materials were mixed in a high-sheer twin-screw Brabender Plasticorder at 80 °C for 12 min. Thin strips of Butyl 165 were first added to the Brabender Plasticorder to heat and soften the rubber at 80 °C for 3 min. Next, the two vulcanizing agents (TMTDS and DTDM) were added to the BR and mixed for 9 min at this temperature. After a total of 12 min of mixing, the master batch was immediately removed from the mixing chamber and quenched on a cold metal surface. After the BR and vulcanizing agents were compounded, a small (approximately 1 g) sample was placed in a heated platen press to form a thin film and then to vulcanize (thermally cross-link) the BR. The hydraulic press was operated with its platens heated to 165 °C, with an applied force of 10 tons. The BR film samples were then cured at 165 °C for 2 h under this applied force and temperature. The films were then cooled and removed and laminated onto Solupor® microporous membrane supports for permeation.

Measurement of test membrane film thickness. The overall thickness of the test membranes was measured using a film thickness measurement device from AMES Masters of Measurement Company. For the hot-pressed LLC–BR films, the amount of infusion through the support and the actual LLC-BR film thickness were measured using EMA imaging of the composite film cross-section with the EMA set to detect certain elements only found in the LLC. For Q-phase and L-phase **2**–BR membranes on Solupor®, elemental P was imaged in the composite film cross-section to determine the extent of **2**-BR penetration through the support and the actual **2**-BR layer thickness. For the H_{II}-phase **1**-BR membranes on Solupor®, the elemental Na found only in monomer **1**, was imaged in the composite film cross-section by EMA to estimate the penetration level and thickness of the LLC layer. See Figures S7 and S8 below for representative cross-sectional EMA elemental imaging pictures. The average measured thicknesses of the test films used in this study are listed in Table S2.

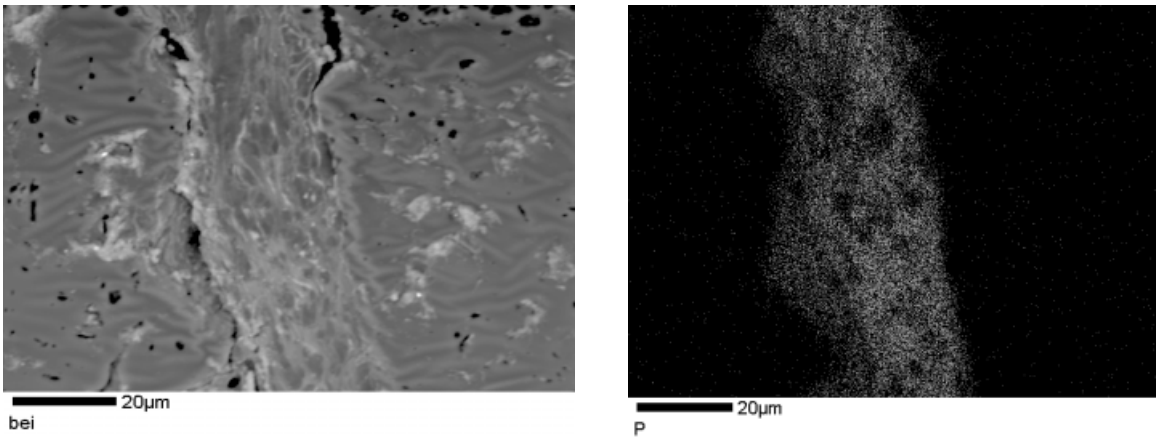

(a) (b)

Fig. S7. (a) Normal mode SEM image of a Q-phase **2**-BR film hot-pressed and cross-linked into Solupor®. The middle vertical region of image is the full membrane cross-section. (b) Same image with the EMA set for elemental P detection (bright regions).

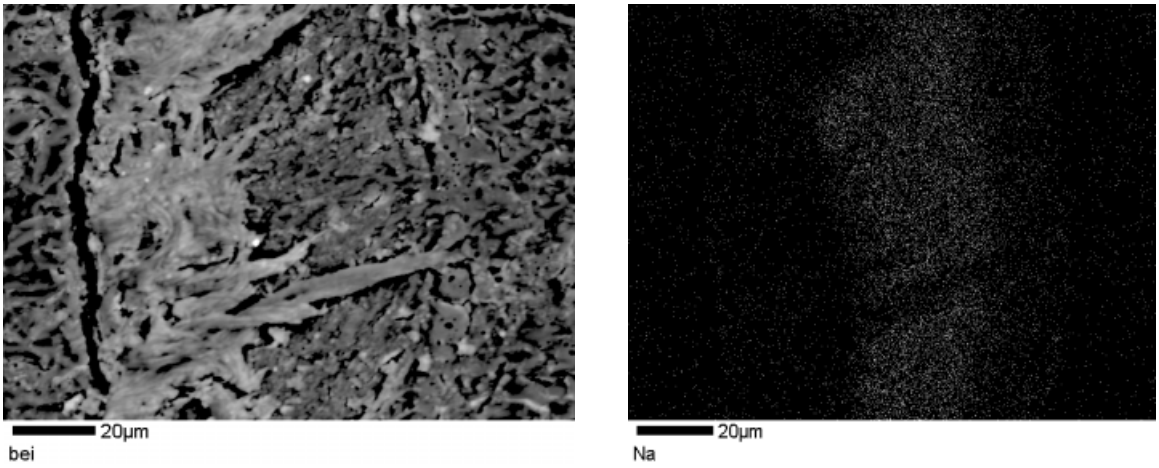

(a) (b)

Fig. S8. (a) Normal mode SEM cross-sectional image of an H_{II}-phase **1**-BR film hot-pressed and cross-linked into Solupor®. The middle vertical region of image is the full membrane cross-section. (b) Same image with EMA set for elemental Na detection (bright regions).

Table S2. The average measured thicknesses of different test membranes.

Membrane:	**Q-phase 2–BR**	**L-phase 2-BR**	**H_{II}-phase 1–BR**	**Pure, cross-linked BR**	**Solupor® support (blank)**
Thickness (μm):	31 ± 3	36 ± 4	31 ± 1	(2.4 ± 2) x 10^2	17.0 ± 0.5

Testing of water vapor permeability of supported, cross-linked LLC-BR membranes. Samples of the supported, cross-linked LLC-BR membranes (3.0 cm O.D.) were mounted into screw-type PVC flanges (1.5 cm I.D.) with one side open to the surrounding atmosphere (71% relative humidity, room temperature), and the other side containing a closed chamber with a known weight of dry desiccant (Drierite). The controlled humidity of the atmosphere was obtained by putting potassium sulfate saturated solution into a tightly sealed glass chamber. The rate of water vapor transport through the testing membrane was determined by measuring the mass increase of the tared dessicant due to water vapor absorption, as a function of time. The background rate of water adsorption onto the PVC flange itself was initially determined, and subsequently subtracted from the observed water vapor permeation of the test samples in the same device. The PVC flanges were always placed into the same surrounding atmosphere for overnight before starting a new water vapor permeation test. This water vapor permeability test is non-destructive, and the membranes used in the above tests were subsequently used for chemical agent vapor permeation tests.

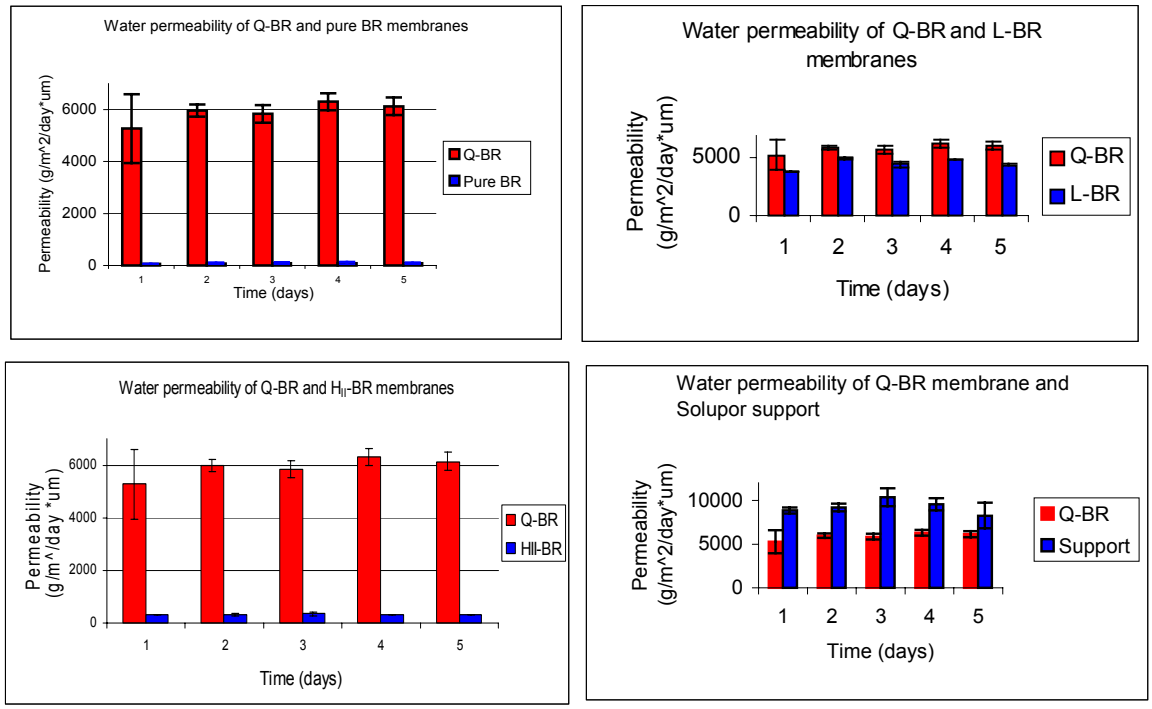

Fig. S9. Water vapor permeability results for: Q-phase **2**-BR membranes vs. pure cross-linked BR membranes (top left); Q-phase **2**-BR membranes vs. L-phase **2**-BR membranes of the same composition (top right); Q-phase **2**-BR membranes vs. H_{II}–phase **1**–BR membranes with the same weight composition (bottom left); and Q-phase **2**-BR membranes vs. blank Solupor® support (bottom right). The data and error bars on the graphs represent the mean and std. dev., respectively, of at least 3 independent runs using different test membranes.

Testing of CEES permeability and measurement of the amount of CEES permeated through the membranes by NMR. Under real-world conditions, the wearer will be perspiring and water vapor will be permeating out of the garment. In the event of a chemical agent attack, the chemical agent vapor will be passing by the outside of the garment. To more accurately simulate these conditions for CEES permeability testing in the laboratory, a permeation cell apparatus was built to flow humid N_2 and saturated chemical agent vapor on opposite sides of the test membranes (Figure S10). CEES and humid air were obtained by flowing dry N_2 into

two bubblers containing CEES and water in one bubbler, and pure water in the other bubbler. The dry N_2 flow rate was controlled to 100 cc min^{-1} on each side of the test membrane. Water was also added to the CEES feed bubbler to balance the water vapor pressure on both sides of the permeation cell to avoid reverse permeation of water vapor. The amount of CEES that permeated through the test membranes to the CEES-free humid N_2 sweep side was collected over activated carbon. Then adsorbed CEES was extracted from the activated carbon by immersing the charcoal in 3 mL of *d*-chloroform in a PTFE and Parafilm sealed glass bottle for at least 16 hours at ambient temperature to achieve the totally desorption of CEES from activated carbon. Then, the amount of CEES permeated was quantified by ^{1}H NMR analysis using 1,3,5-trimethylbenzene as an external standard. *d*-Chloroform was chosen as the extraction solvent because it is miscible with both CEES and 1,3,5-trimethylbenzene, and would rapidly extract CEES from activated carbon. 1,3,5-Trimethylbenzene was chosen because it is nonvolatile, and has simple ^{1}H NMR peaks that do not overlap with those of CEES. The accuracy of this extraction and ^{1}H NMR measurement method was verified by performing control and calibration experiments with known amounts of CEES absorbed onto activated charcoal tubes, and extracted and analyzed in the same manner (Figure S11).

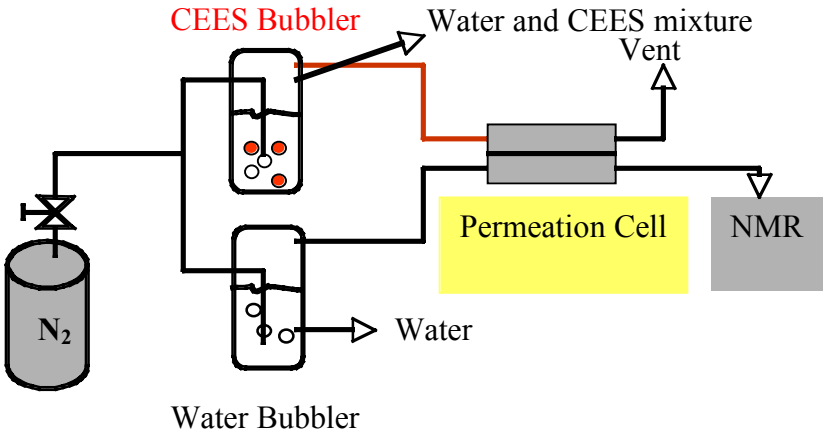

Fig. S10. Schematic of the CEES vapor permeability measurement apparatus.

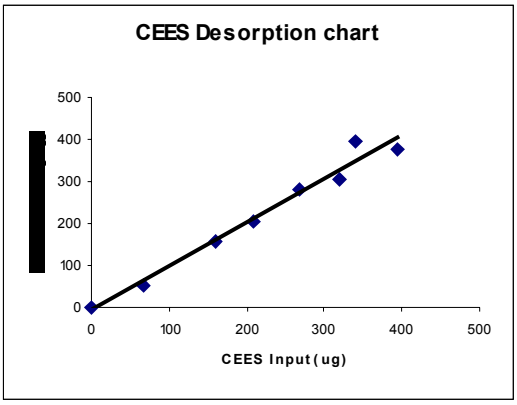

Fig. S11. CEES desorption from activated carbon and NMR analysis calibration chart.

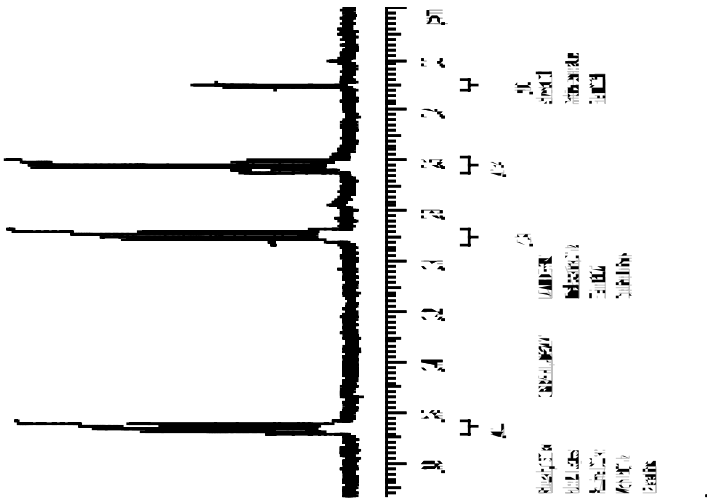

Fig. S12. Representative ^{1}H NMR spectrum of an extracted mixture of CEES and 1,3,5-trimethylbenzene in *d*-chloroform. The ^{1}H-NMR signal of the methylene protons in the –C$\underline{H}_2$–Cl unit in CEES is at δ 3.66, and ^{1}H-NMR signal of the methyl protons (–C$\underline{H}_3$) in 1,3,5-trimethylbenzene is at δ 2.30.

To ensure that all CEES permeated through the test membranes was absorbed onto the activated carbon tubes, we also experimentally determined the CEES absorption saturation point of the

carbon tubes and ensured that all absorbed CEES test values were below this point. The CEES saturation point of the activated carbon collection tubes was found to 83 ± 7 g CEES/tube. For the CEES permeation tests of all the membranes, the total amount of CEES collected in each experiment was far lower than this saturation point.

Testing of water and CEES vapor permeabilities of Q-phase 2-BR membranes exposed to different initial humidity conditions. Water vapor and CEES permeability tests were done on Q-phase **2**-BR membranes exposed to different humidity levels to determine their structural and vapor transport stability. "Wet" or more hydrated membranes were obtained by putting the membranes in 71% relative humidity atmosphere for 24 h. Membranes were kept in a desiccator with 10% relative humidity for 24 h to obtain the "dry" or less hydrated membranes. Water vapor permeability results for the "dry" and "wet" membranes are almost the same as that of the control membranes exposed to ambient humidity levels (Table S3). Normal CEES permeability results showed that "wet" membranes have initially higher CEES permeability, while the "dry" membranes have lower CEES permeability at the beginning of the testing (Table S4 and Fig. S14). This phenomenon may be related to how "open" the phase-separated LLC nanostructure is with different amounts of water/hydration in the material, initially. However, as can be seen from the data in Table S4, once the different hydration-level membranes and their amphiphilic structures equilibrated with the new humidity environment during the 4 h testing period, the CEES permeability values all reach approximately the same value as the ambient humidity "control" membrane. XRD analysis of these different humidity membranes (Table S5) and also of membranes exposed to dynamic vacuum for 24 h (see Fig. S16) (all samples immediately sandwiched and sealed between Mylar sheets to maintain humidity levels during XRD), showed that the Q-phase nanostructure to be intact. These preliminary control experiments show that the nanostructure and selective vapor transport properties of these Q-phase **2**-BR membranes on are extremely stable and resilient to changes in external humidity, both of which are desirable for an operational protective garment material.

Table S3. Water vapor permeability results [g m^{-2} day^{-1} μm] of Q-phase **2**-BR membranes exposed to different initial humidity conditions.

"Dry" membranes (10% rel. humidity)	**"Wet" membranes (71% rel. humidity)**	**"Ambient" membranes (50% rel. humidity)**
$(6.0 \pm 0.3) \times 10^3$	$(6.3 \pm 0.4) \times 10^3$	$(5.9 \pm 0.3) \times 10^3$

Table S4. CEES vapor permeability results [g m^{-2} day^{-1} μm] of Q-phase **2**-BR membranes exposed to different initial humidity conditions.

Time (min)	**"Dry" membranes (10% rel. humidity)**	**"Wet" membranes (71% rel. humidity)**	**"Ambient" membranes (50% rel. humidity)**
10	81 ± 3	$(1.0 \pm 0.1) \times 10^3$	$(2.9 \pm 0.4) \times 10^2$
60	$(1.2 \pm 0.1) \times 10^2$	$(0.8 \pm 0.1) \times 10^3$	$(2.9 \pm 0.1) \times 10^2$
240	$(3.4 \pm 0.5) \times 10^2$	$(0.3 \pm 0.1) \times 10^3$	$(2.8 \pm 0.1) \times 10^2$
360	$(2.7 \pm 0.4) \times 10^2$	$(3.7 \pm 0.1) \times 10^2$	$(2.7 \pm 0.2) \times 10^2$

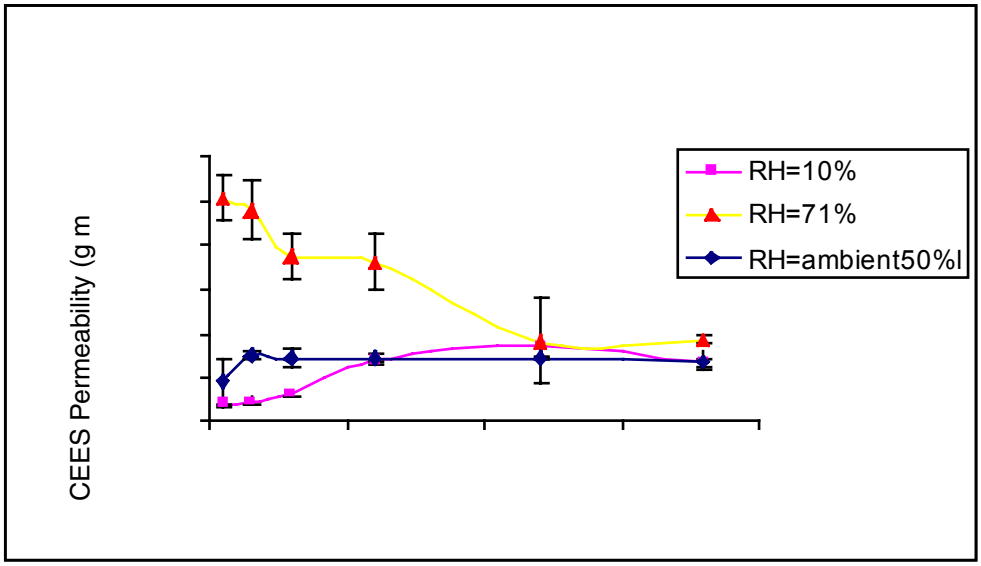

Fig. S14. Plots of CEES vapor permeability vs. time for supported Q-phase **2**-BR membranes that were exposed to different initial humidity conditions. Testing conditions: humid CEES vapor flow on one side of the test membrane, and humid N_2 sweep on the other side.

The increased permeability of the Q-phase **2**-BR membrane to hydrophobic CEES vapor under more humid (i.e., 71% relative humidity) conditions is counter-intuitive because it would be expected that more water uptake in the composite membrane should not affect hydrophobic CEES transport, or block it more. Additional control experiments were performed to determine if this observed initial higher CEES permeability with higher humidity arises from the water-containing LLC part, or the cross-linked BR component and/or hydrophilic Solupor® support in these composite membranes. Control studies with pure (i.e., LLC-free), cross-linked BR on Solupor® support show an even higher initial CEES vapor permeability with high initial external humidity levels (Fig. S15). Consequently, it appears this higher CEES transport with high external humidity is an artifact of the cross-linked BR domains and/or the hydrophilic Solupor® E075-9H01A support material, not the LLC domains. It may be that that high initial external humidity causes the cross-linked BR regions and/or more likely the hydrophilic Solupor® E075-

9H01A fiber matte support to undergo subtle changes in bulk morphology or porosity to let the CEES pass through more easily.

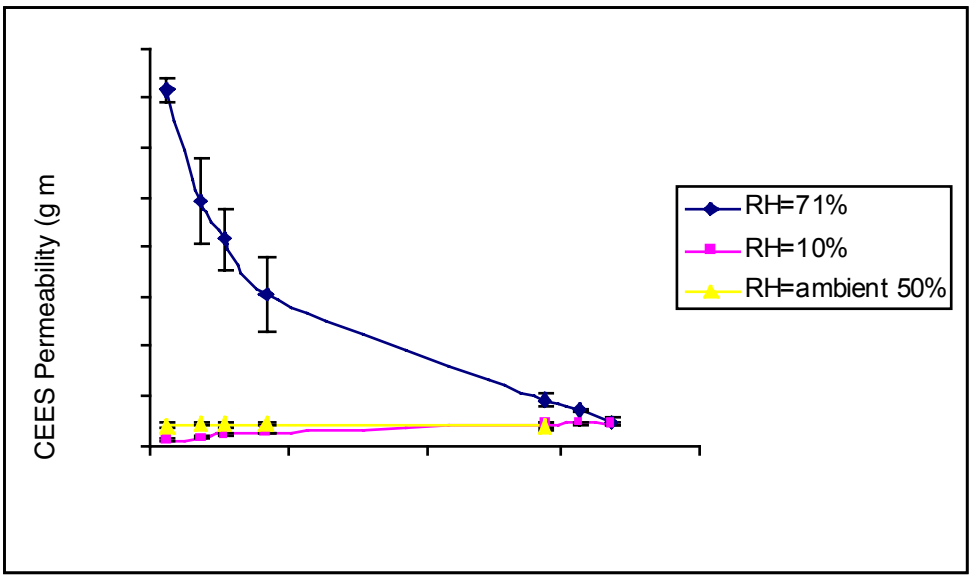

Fig. S15. Plots of CEES vapor permeability vs. time for pure, cross-linked (vulcanized) BR membranes on Solupor® E075-9H01A support that were exposed to different initial humidity conditions. Testing conditions: humid CEES vapor flow on one side of the test membrane, and humid N_2 sweep on the other side.

Table S5. XRD results of *free-standing* Q-phase **2**-BR films of the same composition maintained at different humidity conditions.

2-BR Membrane (% rel. humidity)	**Q-phase XRD d-spacing peaks (Å)**	
	1/√6 peak	**1/√8 peak**
"Wet" (71%)	32.7 ± 0.9	28.5 ± 0.4
"Ambient" (50%)	31.6 ± 0.3	28.0 ± 0.2
"Dry" (10%)	31.1 ± 0.1	27.4 ± 0.3

Water and CEES vapor permeability of Q-phase 2-BR membranes that were dried in vacuo and tested under dry conditions that might dehydrate the membranes. The Q-phase **2**-BR LLC membranes were tested under conditions that might actually dry out the membrane to see if they would still be able to function under these extreme operating conditions. Permeation tests were performed on samples of **2**-BR membranes that were dried in vacuo (50 mtorr) for 24 hours at ambient temperature to see (1) if the LLC structure would collapse; and (2) if the water vapor and CEES vapor permeability and selectivity were detrimentally affected. It was found that such treatment did not affect the LLC nanostructure, as determined by XRD analysis (Fig. S16). It was also not possible to completely dehydrate the **2**-BR membranes even after exposure to dynamic vacuum for 24 h. The water vapor permeability of these "vacuum-exposed" membranes did not decrease to any significant extent compared to before vacuum treatment (Table S6). Also, the CEES permeability of the "vacuum-exposed" membranes under dry CEES testing conditions was found to be much lower than that of the pristine membranes (i.e., either the CEES vapor flow was water-free during testing, or both the CEES vapor and the N_2 sweep on the other side of the test membrane were dry) (Table S7). In fact, when tested with dry CEES vapor flow on one side of the membrane and humid N_2 flow on the other side, these "vacuum-exposed" **2**-BR membranes exhibited substantially higher water/CEES molar selectivity than pristine membranes tested under regular conditions with water vapor present on both the CEES and sweep sides (See Table 1 in manuscript). Consequently, the Q-phase LLC membranes do not fail, nor does their water vapor permeability or water/CEES selectivity suffer under conditions that would normally dehydrate most materials. Unfortunately, we could not do the same permeation experiments at high temperatures that might also dry out the membrane, because the design of our permeation apparatus does not permit variable temperature testing.

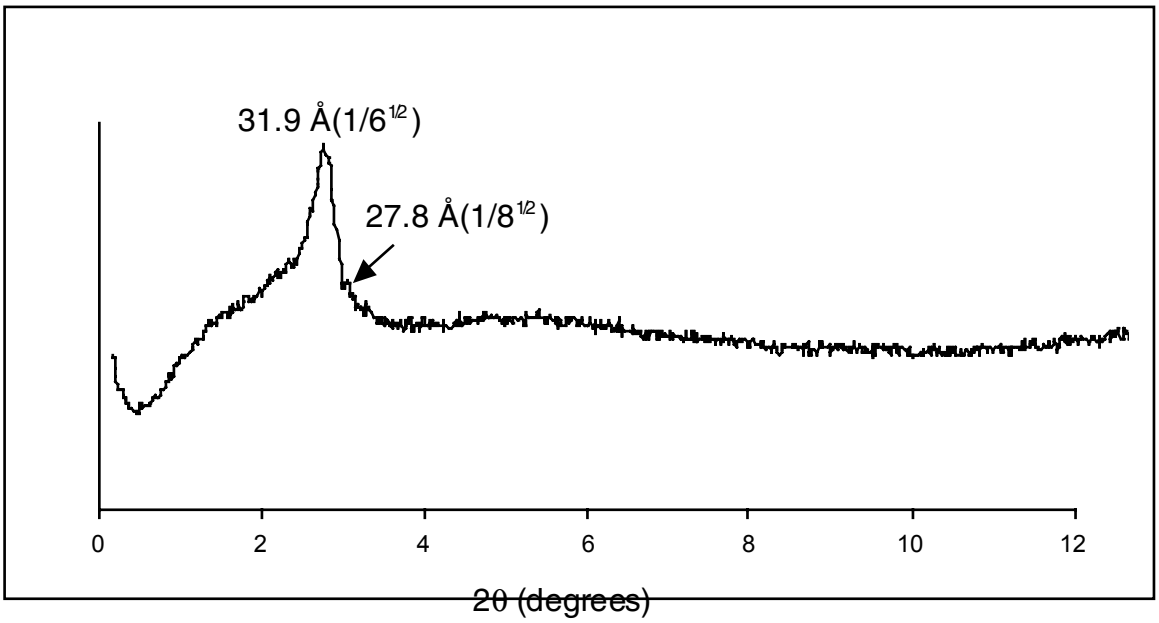

Fig. S16. XRD profile of a cross-linked Q-phase **2**-BR membrane 73.9/9.0/16.2/0.9 (w/w/w/w) **2**/BR/H_2O/photo-initiator) after exposure to dynamic vacuum (50 mtorr) for 24 h at ambient temperature.

Table S6. Comparison of CEES vapor permeability results [g m^{-2} day^{-1} μm] of Q-phase **2**-BR membranes exposed to different initial humidity conditions, against those dried in vacuo (50 mtorr) for 24 h at ambient temperature.

"Dry" membranes (10% rel. humidity)	**"Wet" membranes (71% rel. humidity)**	**"Ambient" membranes (50% rel. humidity)**	**"Vacuum-exposed" membranes (24 h, 50 mtorr, 21 °C)**
$(6.0 \pm 0.3) \times 10^3$	$(6.3 \pm 0.4) \times 10^3$	$(5.9 \pm 0.3) \times 10^3$	**$(6.3 \pm 0.4) \times 10^3$**

Table S7. CEES permeability results [g m^{-2} day^{-1} μm] of ambient Q-phase **2**-BR membranes, and those dried in vacuo (50 mtorr) for 24 h at ambient temperature, when tested under dry CEES flow test conditions.

"Ambient" Q-phase 2-BR membranes		**"Vacuum-exposed" Q-phase 2-BR membranes**	
Dry CEES/dry N_2 flow test conditions	**Dry CEES/humid N_2 flow test conditions**	**Dry CEES/dry N_2 flow test conditions**	**Dry CEES/humid N_2 flow test conditions**
$(2.0 \pm 0.2) \times 10^1$	$(7 \pm 1) \times 10^1$	Not detectable	5.3 ± 0.3

Table S8. Water/CEES vapor molar selectivities of "ambient" Q-phase **2**-BR membranes, and those dried in vacuo (50 mtorr) for 24 h at ambient temperature, when tested with dry CEES flow on one side of the membranes and humid N_2 flow on the other (i.e., sweep) side.

Q-phase 2-BR "Ambient" membranes	**Q-phase 2-BR "Vacuum-exposed" membranes**
$(5.7 \pm 0.1) \times 10^2$	$(8.2 \pm 0.1) \times 10^3$

Determination of the amount of water in the supported, Q-phase 2-BR membranes, and the change in water content under different humidity conditions. The amount of water in the supported LLC-BR membranes under "dry" (i.e., 10% relative humidity) and "wet" (i.e., 71% relative humidity) conditions, was determined by gravimetric analysis using a microgram balance via comparison to the weights of the initial membranes prepared under ambient (50% relative humidity) conditions (Tables S9 and S10). In these studies, supported Q-phase **2**-BR membranes of known LLC/BR/water/photo-initiator composition and initial weights were

weighed under ambient conditions, and then after equilibration under 10% and 71% relative humidity conditions. An average ca. 17 wt. % water loss under "dry" (i.e., 10% relative humidity) conditions and a ca. 56 wt. % water gain under "wet" (i.e., 71% relative humidity) in the membranes was observed relative to the amount of water in the original samples under ambient humidity conditions (Table S10). Also, "vacuum-exposed" **2**-BR membranes showed a ca. 21 wt. % water loss compared to the initial membranes. However, it should be noted that these observed water content changes do not indicate where exactly the water losses and gains are occurring in the composite membrane (i.e., the LLC domains, the BR domains, or the hydrophilic Solupor® support?).

Table S9. Estimates of the amount of water in the supported Q-phase **2**-BR membranes under ambient humidity conditions.

Membrane sample number	**Total weight of supported Q-phase 2-BR membrane (mg)**	**Weight of the Solupor® support used (fixed dimensions) (mg)**	**Weight of the Q-phase (2/BR/H_2O/PI) mixture infused into membrane (mg)**	**Initial wt. of water in membrane, based on fixed composition of LLC/BR/water mixture (mg)* (73.9/16.2/9.0/0.9 (w/w/w/w) 2/H_2O/BR/PI)**
Sample 1	15.53	3.88 ± 0.06	11.65 ± 0.06	1.89 ± 0.01
Sample 2	14.15	3.88 ± 0.06	10.27 ± 0.06	1.66 ± 0.01
Sample 3	11.91	3.88 ± 0.06	8.03 ± 0.06	1.30 ± 0.01
Sample 4	10.28	3.88 ± 0.06	6.40 ± 0.06	1.04 ± 0.01

*****Wt. of water in the membrane = (total weight of membrane – weight of Solupor® support) x 16.2%

Table S10. Estimates of the change in the amount of water in the supported Q-phase **2**-BR membranes under different relative humidity conditions.

Membrane sample number	"Dry" 2-BR membranes (10% rel. humidity)		"Wet" 2-BR membranes (71% rel. humidity)		"Vacuum-exposed" 2-BR membranes (24 h, 50 mtorr)	
	Final weight (mg)	Weight change (mg)	**Final weight (mg)**	**Weight change (mg)**	**Final weight (mg)**	**Weight change (mg)**
Sample 1	15.17	–0.36	16.57	+1.04	15.13	–0.40
Sample 2	13.88	–0.27	15.03	+0.88	13.82	–0.33
Sample 3	11.71	–0.20	/	/	11.63	–0.28
Sample 4	/	/	10.90	+0.62	/	/
% water wt. change in sample (mg /mg water in membrane) (%)	–(1.7 ± 0.2) x 10^1		+(5.6 ± 0.4) x 10^1		–(20.9 ± 0.9)	

Testing for CEES degradation in the presence of water during permeation testing. It is reported in the literature that CEES can slowly hydrolyze in the presence of water to form 2-hydroxyethyl ethyl sulfide (HEES).[6] We looked for HEES content in the CEES-water mixtures on the feed side, and in the collected CEES on the permeate side during permeation testing using ^{1}H NMR, and found that there was very little HEES (–C<u>H$_2$</u>–OH signal: δ 3.75) generated. Consequently, CEES hydrolysis did not affect our testing results at all.

Note on water vapor and chemical agent transport rate requirements in the U.S. military. Military specifications are established for individual products in specific applications. The water vapor transport rate (flux) of 1500 g m^{-2} day^{-1} is generally accepted as the requirement based on typical human respiration.[7] However, opinions vary widely on the desired water vapor transport rate and the maximum allowable chemical agent transport rate for a protective garment material, depending on the authors of these military specifications and the

type of application. That is, discrepancies arise from a lack of a definition for the typical scenario that these protective garments will be used in, currently (i.e., Cold War vs. terrorism). See reference [7] for more details.

Comparison of water vapor and CEES permeability performance of Q-phase 2-BR membranes against commercial cross-linked BR protective gloves currently under evaluation by the Army Research Laboratory (ARL). The water vapor vs. CEES vapor permeability and selectivity of the Q-phase LLC-BR membranes were also compared against that of a commercial cross-linked BR glove material currently being evaluated by the Army Research Laboratories for chemical agent protection. This commercial BR glove material is a chemical protective type III glove material made by Brunswick Corp. that was supplied to us by Dr. Janet Jensen from the ARL:

8415-01-138-2501
GLOVES CHEMICAL
PROTECTIVE,TYPE III
MIL-G-43976C
SMALL LOT(2)
DIA100-91-C-4063
BRUNSWICK CORP.
2-91

This commercial BR glove material contains carbon black (given its black color), as well as other additives. Under the same test conditions as previous described (humid CEES and humid N_2 flow conditions), the Q-phase **2**-BR membranes were found to have over 3 orders of magnitude better water vapor permeability (Fig. S17); ca. 2.8 times better resistance to CEES vapor penetration; and ca. 250 times better water/CEES molar selectivity than this commercial BR glove material (Table S11).

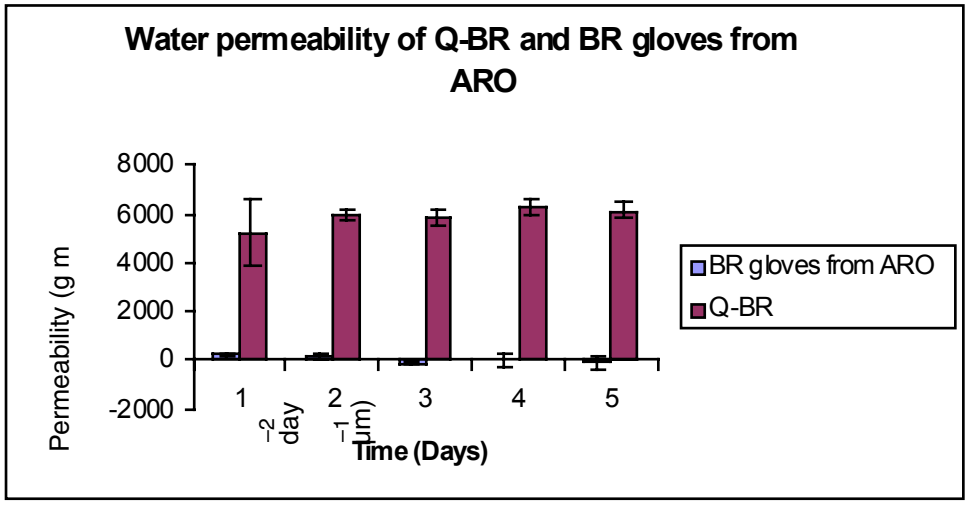

Fig. S17. Comparison of water vapor permeability of Q-phase **2**-BR films and commercial BR gloves under evaluation at the ARL.

Table S11. Water and CEES vapor permeability and molar selectivity of Q-phase **2**-BR membranes and commercial BR gloves under evaluation at the ARL. Testing conditions: humid CEES vapor flow on one side of the test membrane, and humid N_2 sweep on the other side.

Material	**Water Vapor Flux ($g\ m^{-2}\ day^{-1}$)**	**Water Vapor Permeability ($g\ m^{-2}\ day^{-1}\ \mu m$)**	**CEES Vapor Flux ($g\ m^{-2}\ day^{-1}$)**	**CEES Vapor Permeability ($g\ m^{-2}\ day^{-1}\ \mu m$)**	**Water/CEES Molar Selectivity**
Q-phase **2**–BR membrane	$(2.0 \pm 1) \times 10^2$	$(5.9 \pm 0.3) \times 10^3$	9.3 ± 0.4	$(2.86 \pm 0.05) \times 10^2$	**$(1.5 \pm 0.1) \times 10^2$**
BR gloves from ARL	0.28 ± 0.5	$(0.1 \pm 0.1) \times 10^3$	3.2 ± 0.8	$(8 \pm 2) \times 10^2$	**0.6 ± 0.2**

Thickness of Brunswick BR gloves from ARL: $(2.6 \pm 0.2) \times 10^2$ μm
Thickness of supported Q-phase **2**-BR films: 31 ± 3 μm

References for Supplementary Information:

[1] R. C. Smith, W. M. Fischer, D. L. Gin, *J. Am. Chem. Soc.* **1997**, *119*, 4092.

[2] B. A. Pindzola, J. Jin, D. L. Gin, *J. Am. Chem. Soc.* **2003**, *125*, 2940.

[3] See: Cowie, J. M. G. *Polymers: Chemistry & Physics of Modern Materials, 2nd ed.*; Nelson Thornes: Cheltenham, UK, 2001, pp 157–165.

[4] J. Jin, V. Nguyen, W. Gu, X. Lu, B. J. Elliott, D. L. Gin, *Chem. Mater.* **2005**, *17*, 224.

[5] L. J. Bellamy, *The Infra-red Spectra of Complex Molecules*, Chapman and Hall: London, 1975, pp 38–42.

[6] G. S. Groenwald, J. C. Ingram, A. D. Appelhans, J. E. Delmore, D. A. Dahl, *Environ. Sci. Technol.* 1995, *29*, 2107.

[7] In *Strategies to Protect the Health of Deployed U.S. Forces: Force Protection and Decontamination*; M. A. Wartell, M. T. Kleinman, B. H. Huey, L. M. Duffy, Eds.; National Academy Press: Washington, DC; 1999, Chapter 4, pp. 67–107.